

Graph Signal Processing of Indefinite and Complex Graphs using Directed Variation

Kevin Schultz and Marisel Villafañe-Delgado

Johns Hopkins University Applied Physics Laboratory

11100 Johns Hopkins Road, Laurel, MD, 20723, USA

Kevin.Schultz@jhuapl.edu, Marisel.Villafane-Delgado@jhuapl.edu

Abstract—In the field of graph signal processing (GSP), directed graphs present a particular challenge for the “standard approaches” of GSP to due to their asymmetric nature. The presence of negative- or complex-weight directed edges, a graphical structure used in fields such as neuroscience, critical infrastructure, and robot coordination, further complicates the issue. Recent results generalized the total variation of a graph signal to that of directed variation as a motivating principle for developing a graphical Fourier transform (GFT). Here, we extend these techniques to concepts of signal variation appropriate for indefinite and complex-valued graphs and use them to define a GFT for these classes of graph. Simulation results on random graphs are presented, as well as a case study of a portion of the fruit fly connectome.

I. INTRODUCTION

Given a network represented by a graph, where vertices correspond to components and edges represent some relationship, a *graph signal* is a function or time series defined on the graph vertices. Graph signal processing (GSP) is a developing technique for understanding dynamics evolving on discrete network structures [1], [2]. Recent applications include the analysis of interconnections between components in the brain [3] and the interpretability of deep networks in machine learning [4]. GSP analysis has largely focused on extending signal processing concepts for processing graph signals, which are no longer defined on regular (Euclidean) domains. Most techniques trace their roots to the fields of algebraic signal processing [5] or spectral graph theory [6].

The graph Fourier transform (GFT) is a fundamental operator of graph signals, where now the basis functions and frequencies are defined from the eigenvectors and eigenvalues of a graph matrix (e.g., graph Laplacian), respectively. In fact, for so-called *regular* graphs such as lines, rings, and grids, this approach is identical to the standard discrete Fourier transform with appropriate dimension and boundary conditions. The basic definition of the GFT [1] assumes undirected graphs with positive edges. Recent work developed a practical GFT for directed graphs [7], named digraph GFT (DGFT). In this approach, a DGFT matrix is obtained from optimization methods that aim to obtain graph frequencies as uniformly distributed as possible. They introduce a two-step optimization procedure, which first aims to find the maximum directed variation (DV), a generalization from the total variation (TV).

The second step seeks to minimize a spectral dispersion function, finding basis elements whose distribution of DV is smooth and fall within the achievable frequency range in order to obtain a spread DGFT basis.

For many applications of interest, the underlying network structure is directed or the edge weights can be negative or complex, and then the adjacency matrix is no longer positive and symmetric. Under these conditions, the eigenvectors of the Laplacian L no longer form a valid GFT basis. The work in [7] only considers positive weights, and this is not compatible with the network structure in many applications, such as biological neural networks which are best modeled 1) as directed graphs through pre-synaptic to post-synaptic connections and 2) indefinite (i.e., positive and negative) weighted graphs due to the presence of excitatory and inhibitory neurons. Furthermore, due to Dale’s law [8], each vertex should have only either positive or negative weights leaving it (with few exceptions), imposing additional structure on the graph.

In this paper we extend the work in [7] for directed graphs with positive, negative, or complex weights and/or graph signals. We introduce novel concepts of indefinite directed variation (IDV) and complex directed variation (CDV). Furthermore, we introduce appropriate modifications for the greedy and feasible optimization strategies introduced in [7] based on IDV and CDV.

In the following sections, we first review related work on GSP on directed graphs, in particular focusing on recent results from [7]. Next, we show how these concepts extend to indefinite DGFT (IDGFT) and complex DGFT (CDGFT) to perform GSP on indefinite or complex-weighted graphs and address the necessary modifications to the algorithms in [7]. We exercise these new techniques on a set of randomly generated graphs, and finally perform a case-study of a particular indefinite directed graph that models dynamics in a portion of the fruit fly connectome.

II. BACKGROUND

In the most basic framework of GSP, we are given a positive-weighted, undirected graph $\mathcal{G} = (\mathcal{V}, \mathbf{A})$, where \mathcal{V} is the set of vertices with $|\mathcal{V}| = N$ and $\mathbf{A} \in \mathbb{R}^{N \times N}$ is the adjacency matrix of \mathcal{G} with $A_{ij} \geq 0$. Additionally, a real valued function $\mathbf{x} : \mathcal{V} \rightarrow \mathbb{R}^N$ is defined on the vertices of \mathcal{G} . A common approach [1] is to project \mathbf{x} onto the eigenvectors of the graph Laplacian $\mathbf{L} \triangleq \mathbf{D} - \mathbf{A}$, where \mathbf{D} is the diagonal degree matrix, i.e., $D_{ii} = \sum_j A_{ji}$.

When \mathbf{A} is nonnegative-symmetric, the eigenvalues λ_i of \mathbf{L} satisfy $0 = \lambda_1 < \lambda_2 \leq \dots \leq \lambda_N$ and the corresponding eigenvectors v_i are linearly independent. This leads to the analogy that λ_i corresponds to frequency and v_i corresponds to the Fourier harmonics. Letting $V = [v_1, \dots, v_N]$ defines a GFT $\tilde{\mathbf{x}} = V^\top \mathbf{x}$, that reduces to the classical discrete time Fourier transform when \mathcal{G} is an unweighted ring graph. This insight is the intuition for further analogues from classical signal processing.

When the graph \mathcal{G} is directed, this basic formulation using \mathbf{L} breaks down. First, there is no uniform definition of a Laplacian for a directed graph. Some of these extensions may not produce evenly dispersed graph frequencies, as shown in [7], and others may produce degenerate eigenspaces. A more general approach is to use the Jordan decomposition [9], but this is numerically unstable and can produce transforms that do not properly preserve the notion of DC signals nor the overall energy (i.e., is a non-unitary transformation).

An alternative motivation for defining a set of transform basis vectors and a corresponding notion of frequency for directed, nonnegative graphs was developed in [7]. This generalized the notion of the TV of a signal defined on an undirected, nonnegative graph defined as

$$\text{TV}(\mathbf{x}) = \mathbf{x}^\top \mathbf{L} \mathbf{x} = \sum_{i,j=1, j>i}^N A_{ij} (x_i - x_j)^2. \quad (1)$$

The primary insight is that $\text{TV}(\mathbf{v}_i) = \lambda_i$ for eigenvectors of \mathbf{L} and that the right hand side of the expression is amenable to generalization for the case of nonnegative directed graphs. To this end, [7] introduces the concept of DV which is defined as

$$\text{DV}(\mathbf{x}) = \sum_{i,j=1}^N A_{ij} [x_i - x_j]_+^2, \quad (2)$$

where $[x]_+ = \max\{0, x\}$. Note that for undirected graphs $\text{DV}(\mathbf{x}) = \text{TV}(\mathbf{x})$. The intuition behind this quantity is that if directed edges of a graph \mathcal{G} represent the directed flow of a signal from higher values to lower ones, only net positive signal flows will contribute to DV.

Having motivated DV, [7] used intuition from TV to define the graph frequency of a unit vector \mathbf{u} as $f \triangleq \text{DV}(\mathbf{u})$, and thus for an arbitrary orthogonal matrix \mathbf{U} , a directed GFT is defined as $\hat{\mathbf{x}} = \mathbf{U}^\top \mathbf{x}$, which is associated with a set of frequencies f_k corresponding to each column \mathbf{u}_k through $f_k = \text{DV}(\mathbf{u}_k)$. The majority of [7] then focuses on optimization routines for finding \mathbf{U} that result in frequency components f_k that are evenly spread.

III. DIRECTED VARIATION FOR INDEFINITE AND COMPLEX GRAPHS

A. Indefinite Directed Variation

Unlike the work of [7] which focused primarily on approaches for analyzing graph functions on directed graphs with $A_{ij} \geq 0$, in this section we first focus on adapting the techniques of [7] to the case where A_{ij} can be both positive and negative, and $A_{ij} \neq A_{ji}$. In this case, the Laplacian can have both negative, positive, or complex eigenvalues and

non-orthogonal eigenvectors. This suggests that we need to adapt DV to properly account for the variation introduced by the negative components of A_{ij} . The natural adaptation is to extend DV to IDV via

$$\text{IDV}(\mathbf{x}) = \sum_{i,j=1}^N [A_{ij}]_+ [x_i - x_j]_+^2 + [A_{ij}]_- [x_i - x_j]_-^2 \quad (3)$$

where $[x]_- = -\min\{0, x\}$. This is equivalent to DV for positive (or negative) directed graphs, and thus is equivalent to TV for undirected graphs.

1) *Complex DV*: Note that the definition of IDV is readily extendable to a notion of directed variation for analysis when the graph signal or the directed adjacency matrix has complex values. Example use cases include multi-agent systems [10], infrastructure networks [11], and neural networks [12]. Let $\text{Re}(\cdot)$ and $\text{Im}(\cdot)$ denote the real and imaginary parts of the argument, respectively, and for complex \mathbf{A} and \mathbf{x} let

$$\tilde{\mathbf{y}} = \begin{bmatrix} \text{Re}(\mathbf{A}) & -\text{Im}(\mathbf{A}) \\ \text{Im}(\mathbf{A}) & \text{Re}(\mathbf{A}) \end{bmatrix} \begin{bmatrix} \text{Re}(\mathbf{x}) \\ \text{Im}(\mathbf{x}) \end{bmatrix} \triangleq \tilde{\mathbf{A}} \tilde{\mathbf{x}} \quad (4)$$

and then

$$\mathbf{A} \mathbf{x} = \tilde{\mathbf{y}}_{1:N} + i \tilde{\mathbf{y}}_{N+1:2N}, \quad (5)$$

where the subscripts indicate the first and second N dimensions of \mathbf{y} , respectively. This equivalence between complex and real matrix algebras offers an immediate generalization of DV to the case of complex graphs and graph signals by defining the CDV of a complex signal as the IDV of the associated real valued adjacency matrix and graph signal. Formally, given a complex, directed adjacency matrix \mathbf{A} and graph signal \mathbf{x} , define

$$\begin{aligned} \text{CDV}(\mathbf{x}) &= \sum_{i,j=1}^{2N} [\tilde{A}_{ij}]_+ [\tilde{x}_i - \tilde{x}_j]_+^2 + [\tilde{A}_{ij}]_- [\tilde{x}_i - \tilde{x}_j]_-^2 \\ &= \sum_{i,j=1}^N [\text{Re}(A_{ij})]_+ [\text{Re}(x_i - x_j)]_+^2 + [\text{Re}(A_{ij})]_- [\text{Re}(x_i - x_j)]_-^2 \\ &\quad + [\text{Re}(A_{ij})]_+ [\text{Im}(x_i - x_j)]_+^2 + [\text{Re}(A_{ij})]_- [\text{Im}(x_i - x_j)]_-^2 \\ &\quad + [\text{Im}(A_{ij})]_- [\text{Re}(x_i) - \text{Im}(x_j)]_+^2 \\ &\quad + [\text{Im}(A_{ij})]_+ [\text{Re}(x_i) - \text{Im}(x_j)]_-^2 \\ &\quad + [\text{Im}(A_{ij})]_+ [\text{Im}(x_i) - \text{Re}(x_j)]_+^2 \\ &\quad + [\text{Im}(A_{ij})]_- [\text{Im}(x_i) - \text{Re}(x_j)]_-^2 \end{aligned} \quad (6)$$

B. Minimizing Spectral Dispersion

Two methods for optimizing the spread of DV were introduced in [7]. The first, called the *feasible* method, used gradient descent on Stiefel manifolds [13] which can be computationally prohibitive due to the matrix decompositions for large graphs, as well nonconvexity of the overall optimization problem requiring multiple initial conditions for the gradient descent. As an alternative, [7] also introduced a *greedy* heuristic that exploits submodularity which is both highly efficient and uses basis vectors of a related undirected graph (this latter fact is desirable as the resulting graph transform will be in a basis that is in some sense “natural”). Next, we will discuss modifications to these two approaches that are necessary to use IDV and CDV in place of DV.

1) *Feasible Gradient Descent Approach*: The feasible gradient descent approach for minimizing spectral dispersion using IDV proceeds almost identically to what is described in [7]. The main differences are to replace DV with IDV in the objective function computations. This also changes the gradient computations, with the only substantial change occurring to the single vector gradient \tilde{g}_i defined in [7, Eq. (15)]. From the linearity of the derivative, in the case of IDV this becomes

$$\begin{aligned} \tilde{g}_i = 2 \left(& [\mathbf{A}_{\cdot i}^\top]_+ [\mathbf{u} - u_i \mathbf{1}_N]_+ - [\mathbf{A}_{\cdot i}]_+ [u_i \mathbf{1}_N - \mathbf{u}]_+ \\ & - [\mathbf{A}_{\cdot i}^\top]_- [\mathbf{u} - u_i \mathbf{1}_N]_- + [\mathbf{A}_{\cdot i}]_- [u_i \mathbf{1}_N - \mathbf{u}]_- \right) \end{aligned} \quad (7)$$

to use the notation of [7].

An extension of the gradient descent approach for CDV is also straight-forward. We can compute the single-vector complex gradient of the now complex vector by using the same complex-to-real transform used to derive CDV from IDV. For a complex adjacency matrix \mathbf{A} and vector \mathbf{u} (and transformed real-valued $\tilde{\mathbf{A}}$ and $\tilde{\mathbf{u}}$) we can define an associated real-valued gradient $\tilde{\tilde{g}}$ by

$$\begin{aligned} \tilde{\tilde{g}}_i = 2 \left(& [\tilde{\mathbf{A}}_{\cdot i}^\top]_+ [\tilde{\mathbf{u}} - \tilde{u}_i \mathbf{1}_{2N}]_+ - [\tilde{\mathbf{A}}_{\cdot i}]_+ [\tilde{u}_i \mathbf{1}_{2N} - \tilde{\mathbf{u}}]_+ \\ & - [\tilde{\mathbf{A}}_{\cdot i}^\top]_- [\tilde{\mathbf{u}} - \tilde{u}_i \mathbf{1}_{2N}]_- + [\tilde{\mathbf{A}}_{\cdot i}]_- [\tilde{u}_i \mathbf{1}_{2N} - \tilde{\mathbf{u}}]_- \right) \end{aligned} \quad (8)$$

and then the complex gradient is $\tilde{g} = \tilde{\tilde{g}}_{1:N} + i\tilde{\tilde{g}}_{N+1:2N}$. The remaining changes to gradient descent approach are handled by taking the appropriate inner product on the complex space (i.e., using conjugate transpose instead of transpose), as outlined in the original reference [14, Sec. 4.2] to the feasible method used by [7].

2) *Greedy Heuristic Approach*: Due to the computational complexity and non-convexity of the gradient descent approach, [7] introduced a greedy heuristic that uses the Laplacian of a corresponding undirected graph. Specifically, from a positive directed graph $\mathcal{G} = (\mathcal{V}, \mathbf{A})$ they define the *underlying undirected graph* $\mathcal{G}^u = (\mathcal{V}, \mathbf{A}^u)$ where $A_{ij}^u = \max\{A_{ij}, A_{ji}\}$. Since \mathcal{G}^u is symmetric, the corresponding Laplacian \mathbf{L}^u will have orthogonal eigenvectors and can be used for a directed GFT. An additional motivation for considering \mathcal{G}^u is that $\text{DV}(\mathbf{x})$ (with respect to \mathcal{G}) is bounded by λ_{max}^u , the maximum eigenvalue of \mathbf{L}^u . Noting that for directed graphs $\text{DV}(\mathbf{x}) \neq \text{DV}(-\mathbf{x})$, the authors use a greedy search over the collection $\{\pm \mathbf{v}_i\}$ for \mathbf{v}_i eigenvectors of \mathbf{L}^u that chooses only one from $\pm \mathbf{v}_i$ for each i . This relies on a proof of submodularity of the spread of DV derived using matroid theory.

In the case of IDV, we use the underlying graph with adjacency matrix $\mathbf{A}^{[u]} = \max\{|A_{ij}|, |A_{ji}|\}$ and the eigenvectors of the corresponding Laplacian $\mathbf{L}^{[u]}$. The matroid conditions still hold, as the basis elements of $\mathbf{L}^{[u]}$ are orthonormal. Thus, the spread of IDV will also be submodular, and the greedy optimization of IDV spread can proceed as described in [7], albeit with the substitution of IDV in place of DV. The presence of complex weights presents an additional wrinkle in the greedy optimization approach. In the complex case, we should instead consider the effect of an arbitrary unit-norm complex

scalar $e^{i\theta}$ on the basis vectors, as opposed to simply ± 1 . This presents a scalar-argument continuous optimization problem that must be computed for each basis vector at each time step of the greedy approach. Furthermore, this optimization is not convex so will require several initial conditions to find the global minimum in a gradient descent approach. As an alternative, we propose instead to compute initially the CDV of each basis vector multiplied by $e^{i\theta_k}$ for θ_k evenly spaced on a grid between $[0, 2\pi)$ and then proceeding with the greedy algorithm, with the selection made over rotation angles θ_k as opposed to only ± 1 .

IV. RESULTS

A. Simulation Results

We performed the following experiment to assess the impact of using the appropriate notion of DV. We considered ring lattice networks with $N = 16$ nodes and degree 2, Erdos Renyi networks with $N = 16$ nodes and probability of attachment $p = 0.2$, and stochastic block networks with three communities and $N_c = 8$ nodes per community. All edges were directed with weights uniformly drawn from $\{\pm 1, \pm i\}$. For each of these graphs \mathcal{G} , we created an indefinite graph \mathcal{G}_I by replacing the $\pm i$ edges with ± 1 , and a positive graph \mathcal{G}_P by setting all weights to 1. For 10,000 random instances of the above classes, we generated two random unit vectors in \mathbb{R}^N and compared the resulting DVs using \mathcal{G}_P to the IDVs using \mathcal{G}_I and the CDVs using \mathcal{G} . Across all 60,000 comparisons we found that the relative orderings of the two vectors were different greater than 35% of the time. This highlights the importance of IDV or CDV, as the frequency interpretation of a given basis element or signal can change substantially.

To further understand the proposed methods we compared them on a subset of $M = 20$ for graph class above. Fig. 1a shows box-plots of the maximum IDV and CDV, indicating that the feasible method increases DV beyond the greedy method. Furthermore, these show that distributions of particular classes of graphs can vary widely. Unlike maximum DV, it is essentially impossible to directly compare dispersion, defined as $\delta_{IDV}(\mathbf{U}) = \sum_{i=1}^{N-1} [\text{IDV}(\mathbf{u}_{i+1}) - \text{IDV}(\mathbf{u}_i)]^2$ (and similarly δ_{CDV}) as dispersion is strongly correlated with maximum DV (see Fig. 1b), meaning the feasible method also tends to produce an increase in dispersion, despite a qualitatively smoother distribution. That said, each graph class does tend to produce relatively similar dispersions.

B. Fruit Fly Protocerebral Bridge

As biological neural networks were the primary motivator for developing IDV, in this example we consider a model of the fruit fly (*Drosophila melanogaster*) protocerebral bridge (PB) from [15]. This sub-system of the fruit fly brain is thought to be responsible for maintaining heading direction in the navigation process of the fruit fly. The adjacency matrix and graph signals are provided from a recent study [15]. It includes three primary structures, the ellipsoid body (EB) (nodes 0-31), the excitatory portion of the PB (nodes 32-49), and the inhibitory portion of the the PB (nodes 50-59; see Fig. 2 (a)) as well as a simulation that produces ring attractor dynamics

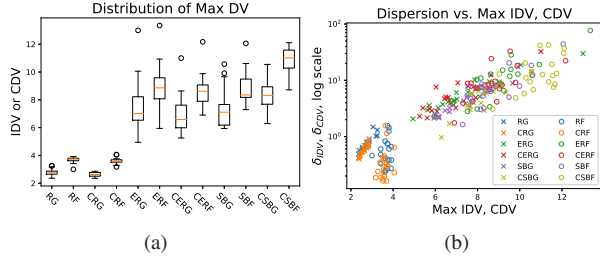


Fig. 1. (a) Distributions of maximum IDV or CDV basis elements. R , ER , and SB denote the graph class, a prefix C denotes complex, and a G or F suffix denotes greedy or feasible method. (b) Scatter plots of dispersion vs. maximum IDV/CDV to illustrate difficulty comparing dispersion between graphs and GFTs.

that we use to define the graph signals in our analysis. The adjacency matrix in Fig. 2 is highly asymmetric, as synaptic signals only flow in one direction, and follows Dale’s Law (i.e., each neuron affects others with only positive or negative weights). An example simulation is shown in Fig. 2b, where the network is initially (0.5 s) subjected to a background noisy spiking current stimulus into the PB, followed by 4 s of background stimulus plus feed-forward stimulus representing constant, periodic rotation of the fly’s heading, followed by another 0.5 s of background stimulus. Other than the repeating stimulus, we use the default parameters from [15].

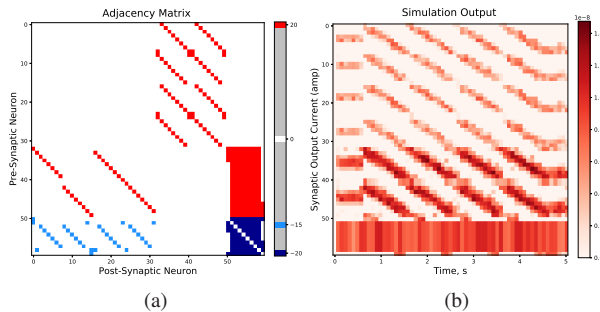


Fig. 2. (a) Adjacency matrix of the fruit-fly PB model from [15]. Note the presence of both excitatory neurons (red) and inhibitory neurons (blue). (b) Sample simulation under noisy fixed frequency rotation stimulus into the PB from 0.5-4.5 s as described in [15]. For presentation purposes, every 833rd sample of the fixed sample time (0.1 ms) simulation is shown.

Fig. 3a shows the resulting IDVs from the greedy and feasible methods. The feasible method results in more even spacing in IDVs compared to the greedy. Comparisons between IDV and DV from greedy methods are shown in Fig. 3b, showing considerable differences in the relative ordering of the identical harmonics despite identical basis elements. This indicates substantially different frequency interpretation under the two measures, and thus the inclusion of negative weights in the graph is meaningful. It is more difficult to directly compare the feasible methods, as the graph harmonics produced are quite different. One clear point of comparison, however, is that between the different “maximum frequency” harmonics produced by the first stage of the feasible method. Table I shows that while the greedy methods agree on the maximum frequency harmonic, the feasible methods produce quite dif-

ferent results. Again, this further illustrates the importance of including both directivity and weight into the GFT.

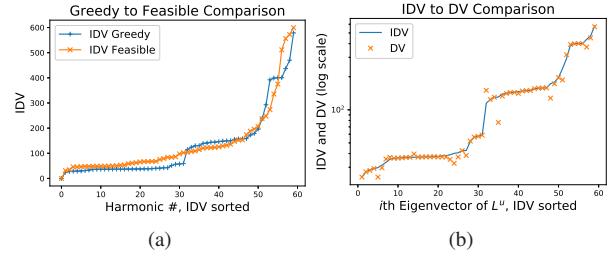


Fig. 3. (a) Comparison of IDV values resulting from greedy and feasible approaches. Note higher maximum and qualitatively smoother (more even) distribution for the feasible method. (b) Comparison of IDV and DV values from greedy methods, sorted by IDV value of corresponding underlying Laplacian eigenvector.

TABLE I
COMPARISON BETWEEN GREEDY AND GRADIENT DESCENT APPROACHES

	Feas. IDV	Greedy IDV	Feas. DV	Greedy DV
Max IDV	599.43	578.48	576.24	578.48
Max DV	559.51	569.86	570.39	569.86
$\delta_{IDV}, \delta_{CDV}$	31286.5	33420.8	28780.3	38559.9

IDGFT matrices generated using the feasible and greedy IDV methods are shown in Fig. 4a and Fig. 4b, respectively, with eigenvectors sorted by IDV. Despite the perceived benefits of the feasible method for this network, we find that the greedy transform more intuitively captures the structure of the network leading to more interpretable graph Fourier analysis, whereas the feasible method spreads the energy more evenly across the different harmonics. Furthermore, the “discontinuities” in the greedy IDV values (Fig. 3a) actually correspond to important functional blocks within the highly structured network considered here.

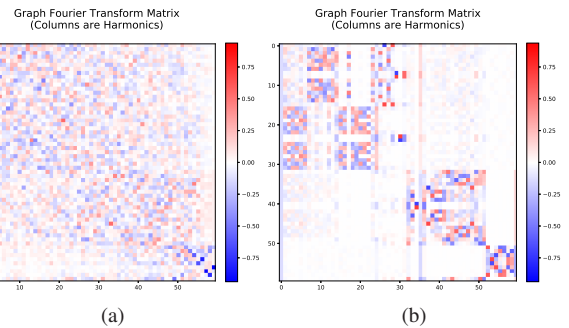


Fig. 4. IDGFT matrices for adjacency matrix in Fig. 2. (a) Feasible gradient descent approach. (b) Greedy submodular approach. While the feasible method produces both a higher maximum IDV and lower overall IDV dispersion, the greedy approach “captures” more of the network structure.

The total GFT power of the graph signal (over time) in Fig. 2b using the two transforms in Fig. 4 is shown in Fig. 5. Using visual inspection in conjunction with the IDV distribution, we have divided the greedy harmonics into four groups as shown in Fig. 5 (bottom). The first grouping includes basis elements 0, 35, and 59 which coarsely measures signal in

the entire network, in the EB (nodes 0-31) vs. the PB (32-59), and the interior inhibitory neurons (51-58) vs. the remainder of the PB. These three elements coarse-grain the signal power into these functional blocks. The second grouping covers spectral content primarily within the the EB. Curiously, the third grouping includes not only the excitatory neurons in the PB, but also the first and last inhibitory neurons, presumably due to the fact that they have a slightly different neighborhood structure from the other inhibitory neurons. This also leads to a fundamentally different graph signal for those boundary neurons, as evident in Fig. 4b. The final group consists of the interior inhibitory neurons which appear to add little additional spectral content to the graph beyond their average (captured in the first group).

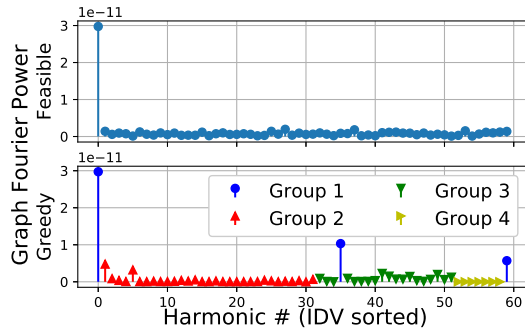


Fig. 5. Power spectra of graph signal from Fig. 2b. Top: Feasible IDV-based transform. Bottom: Greedy IDV-based transform, colored by frequency groupings. Group 1 corresponds to harmonics that capture coarse activity levels between the EB (Group 2), excitatory-PB and boundary inhibitory neurons (Group 3) and interior inhibitory neurons (Group 4).

An interesting facet revealed through this graph Fourier analysis is that the two dominant components in the ellipsoid body, $\hat{x}_1(t)$ and $\hat{x}_5(t)$, result in periodic oscillations (at the input rotation period) that are 90° out of phase (see Fig. 6). As the inputs to the system are in the PB, these dynamics must be driven from there, and indeed we see that the top four components have the same periodic structure (\hat{x}_{41} , \hat{x}_{42} , \hat{x}_{45} and \hat{x}_{49}). Since the EB then feeds back into the PB it would seem to indicate that the EB effectively aggregates and stabilizes several Fourier components and feeds them back in the reciprocal relationship between the EB and the PB.

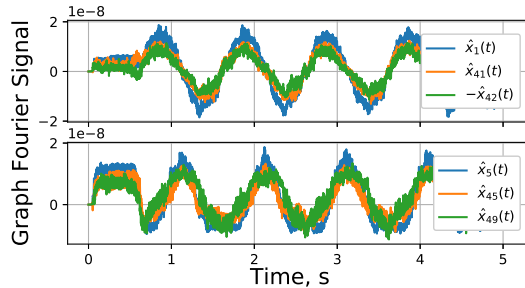


Fig. 6. Fluctuations of projections of graph signals into certain graph harmonics that exhibit periodic behavior consistent with the input rotation rate. Note the bottom signals are 90° out of phase with those in the top. This signals, correspond to peaks in Group 2 and 3 in Fig. 5 and comprise $\approx 20\%$ of the total graph signal power.

V. CONCLUSIONS AND FUTURE WORK

In summary, we have extended the techniques in [7] to develop a GFT that can be used for indefinite- and complex-weighted graphs. We showed that much of the intuition and rationale behind the original DV motivation applies to the transforms presented here. Furthermore, as using only the absolute value of the weights can have a substantial impact on the frequency interpretation of graph harmonics and the resulting analysis, this indicates the need to consider both the sign or phase of the weights in addition to the directionality. Finally, we applied these tools to a simulated biological neural network and were able to apply GFT analysis to derive insight into its dynamics. In future work, we will explore other algorithms and heuristics for the optimization of IDV and CDV, and apply IDGFT and CDGFT to other applications.

ACKNOWLEDGEMENT

We thank Dr. Grace Hwang for pointing us to the fly simulation and for helpful discussions.

REFERENCES

- [1] D. Shuman, S. Narang, P. Frossard, A. Ortega, and P. Vandergheynst, "The emerging field of signal processing on graphs: Extending high-dimensional data analysis to networks and other irregular domains," *IEEE Signal Processing Magazine*, vol. 3, no. 30, pp. 83–98, 2013.
- [2] A. Sandryhaila and J. M. Moura, "Discrete signal processing on graphs," *IEEE transactions on signal processing*, vol. 61, no. 7, pp. 1644–1656, 2013.
- [3] A. Raj, C. Cai, X. Xie, E. Palacios, J. Owen, P. Mukherjee, and S. Nagarajan, "Spectral graph theory of brain oscillations," *bioRxiv*, p. 589176, 2019.
- [4] R. Anirudh, J. J. Thiagarajan, R. Sridhar, and T. Bremer, "Margin: Uncovering deep neural networks using graph signal analysis," *arXiv preprint arXiv:1711.05407*, 2017.
- [5] M. Puschel and J. M. Moura, "Algebraic signal processing theory: Foundation and 1-d time," *IEEE Transactions on Signal Processing*, vol. 56, no. 8, pp. 3572–3585, 2008.
- [6] F. R. Chung and F. C. Graham, *Spectral graph theory*. American Mathematical Soc., 1997, no. 92.
- [7] R. Shafipour, A. Khodabakhsh, G. Mateos, and E. Nikolova, "A directed graph fourier transform with spread frequency components," *IEEE Transactions on Signal Processing*, vol. 67, no. 4, pp. 946–960, 2018.
- [8] J. C. Eccles, "From electrical to chemical transmission in the central nervous system: the closing address of the sir henry dale centennial symposium cambridge, 19 september 1975," *Notes and records of the Royal Society of London*, vol. 30, no. 2, pp. 219–230, 1976.
- [9] A. Sandryhaila and J. M. Moura, "Discrete signal processing on graphs: Frequency analysis," *IEEE Transactions on Signal Processing*, vol. 62, no. 12, pp. 3042–3054, 2014.
- [10] Z. Lin, L. Wang, Z. Han, and M. Fu, "Distributed formation control of multi-agent systems using complex laplacian," *IEEE Transactions on Automatic Control*, vol. 59, no. 7, pp. 1765–1777, 2014.
- [11] J. Sanchez, R. Caire, and N. Hadjsaid, "ICT and electric power systems interdependencies modeling," in *International ETG-Congress 2013; Symposium 1: Security in Critical Infrastructures Today*. VDE, 2013, pp. 1–6.
- [12] E. P. Frady and F. T. Sommer, "Robust computation with rhythmic spike patterns," *Proceedings of the National Academy of Sciences of the United States of America*, vol. 116, no. 36, pp. 18 050–18 059, 2019.
- [13] A. Edelman, T. A. Arias, and S. T. Smith, "The geometry of algorithms with orthogonality constraints," *SIAM journal on Matrix Analysis and Applications*, vol. 20, no. 2, pp. 303–353, 1998.
- [14] Z. Wen and W. Yin, "A feasible method for optimization with orthogonality constraints," *Mathematical Programming*, vol. 142, no. 1-2, pp. 397–434, 2013.
- [15] K. S. Kakaria and B. L. de Bivort, "Ring attractor dynamics emerge from a spiking model of the entire protocerebral bridge," *Frontiers in behavioral neuroscience*, vol. 11, p. 8, 2017.